Hindawi
Geofluids
Volume 2022, Article ID 8524932, 20 pages
https://doi.org/10.1155/2022/8524932

Research Article

Chemical Evolution Process and Quality Assessment of Seepage Groundwater in Tunnel Crossing Gas-Bearing Coal Seams

Yuanming Liu, Chen Peng, Qiaowei Yuan, and Huiyu Chen

School of Civil Engineering, Guizhou University, Guiyang 550000, China

Correspondence should be addressed to Yuanming Liu; liuym_2021@163.com

Received 18 February 2022; Accepted 18 April 2022; Published 16 May 2022

Academic Editor: Yue Niu

The chemical characteristics of groundwater in the gas coal seam section of the tunnel have rich geological significance. To study the chemical evolution process and controlling factors of groundwater in the gas-bearing coal seam section of the tunnel, and the influence of tunnel coal removal on the groundwater quality, field investigations and laboratory experiments were carried out on the groundwater in the coal measure strata and the high-gaseous section and surrounding aquifers. Through hydrochemical analysis, correlation analysis, hydrochemical simulation, and other methods, the chemical origin of groundwater in coal measure strata and other aquifers was revealed. The water quality of groundwater was analyzed by water quality index (WQI), sodium adsorption rate (SAR), percentage of soluble sodium (Na^+%), and participation of sodium carbonate (RSC). The results show that the water samples of each aquifer are weakly alkaline. Influenced by formation lithology and mineral redox reactions, the genesis of coal formation water is more complex than that of natural karst groundwater. The water chemistry characteristics show obvious differences among aquifer groups, with low correlation of HCO_3^-, Ca^{2+}, and Mg^{2+}. The central drainage ditch is dominated by dolomite dissolution, and the sloping shaft side ditch is dominated by calcite dissolution, and ion exchange effects are prevalent in different water sources. In terms of irrigation water quality, the permeability index (PI), magnesium hazard (MH), and Kelly index (KI) calculations show that 45.8% of the water samples are in the "unsuitable" condition. This study helps to fully understand the quality of coal seam water in tunnels and can provide a reference for groundwater utilization.

1. Introduction

At present, more and more tunnels encounter high-gas-developed strata and coal measure strata in the process of excavation, which may pollute the groundwater environment. The interaction between coalbed methane-groundwater-coal-rock and its hydrochemical response is a research hotspot [1–3]. After tunnel excavation, CO_2, CH_4, and other gases adsorbed in the coal seam are dissolved in the groundwater, while various physicochemical reactions occur between the groundwater and the coal seam and surrounding rocks in the runoff process. Also, elements in the coal seam also enter the aquifer through leaching, and the chemical properties of the groundwater in the original aquifer would be influenced.

In the natural state, there is little exchange of water between the coal formation water and the surrounding karst aquifers in the tunnel site area. However, tunnel construction breaks the original hydraulic and chemical balance within the groundwater system, accelerates the groundwater circulation and water-rock interaction between different aquifers [4], and transforms the relative water barrier in a certain range into a permeable layer. As a result, the relatively retained coal formation water is discharged or mixed with other aquifers, which affects the field groundwater system.

Karst groundwater is an important part of the ecosystem in Guizhou Province [5, 6] and is closely related to local human life and economic development. Karst groundwater systems are highly nonhomogeneous due to their unique hydrogeological characteristics, and their water quantity and quality changes are very sensitive to the external environment [7]. Tongzi Tunnel is the first long highway tunnel under construction in Guizhou Province. It needs to pass

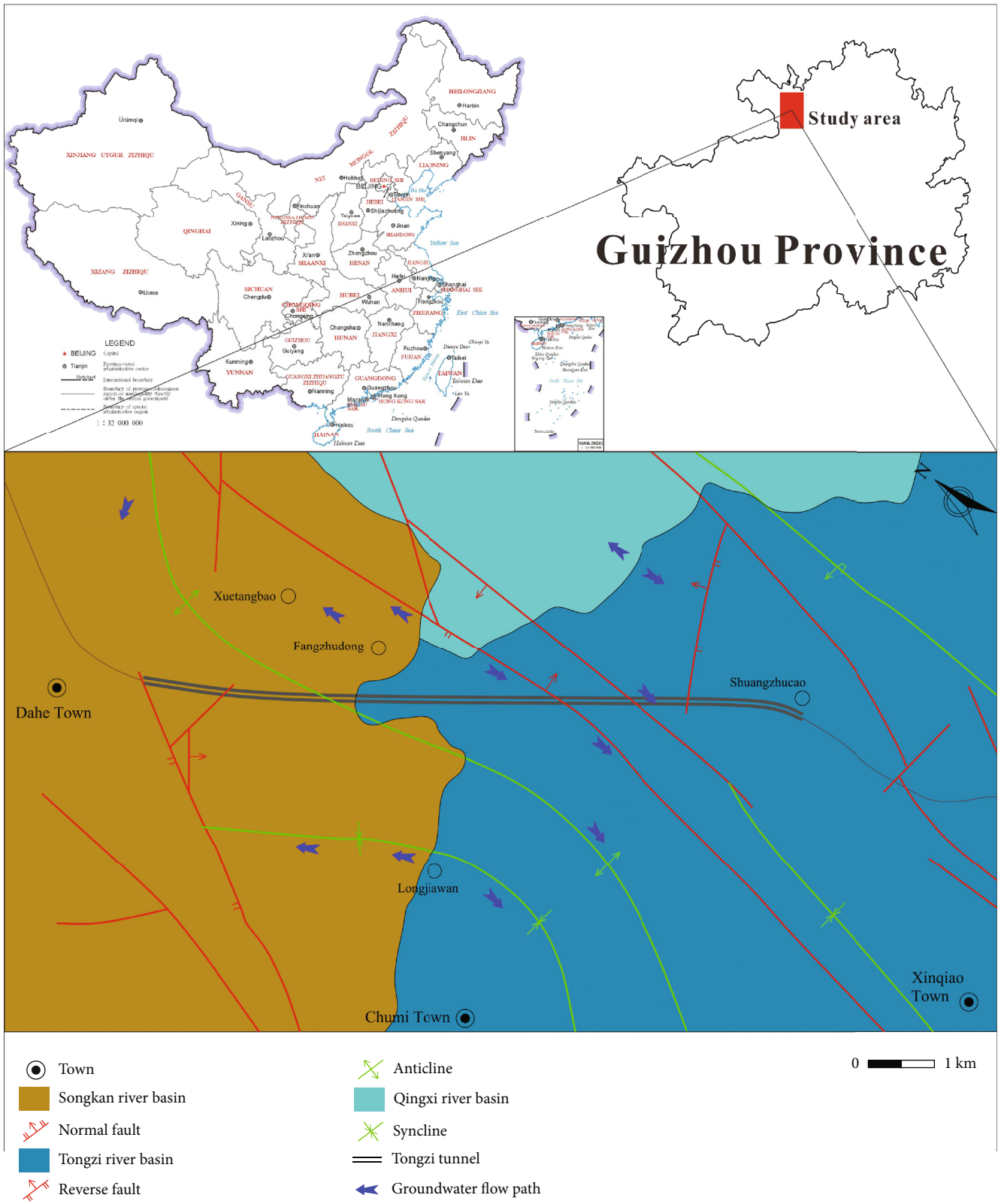

Figure 1: Location and overview of the study area (China map from Ministry of Natural Resources Standard Map System).

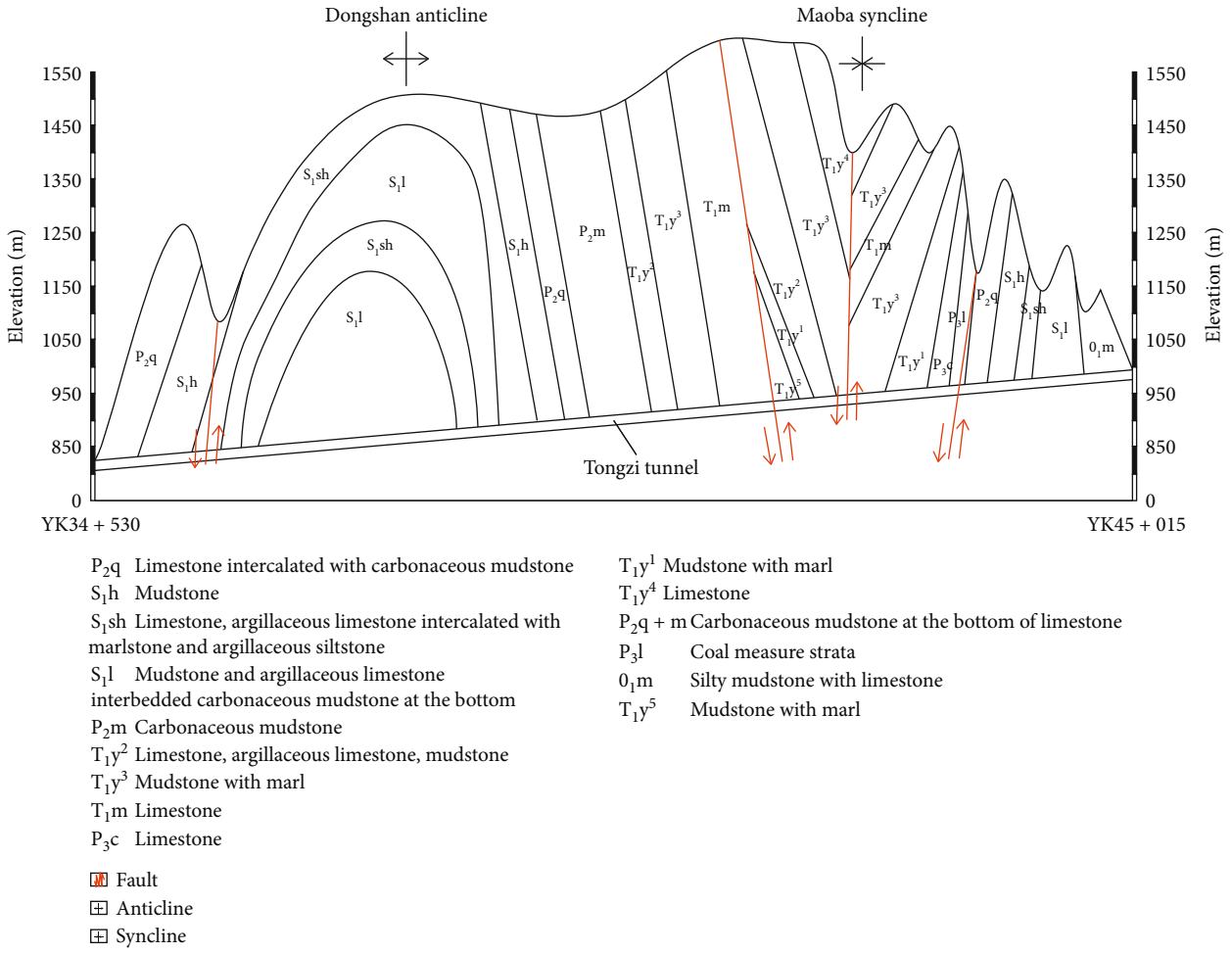

Figure 2: Geological profile of Tongzi Tunnel.

through high gas and coal measure strata during construction. Therefore, revealing the hydrochemical evolution process of groundwater in coal measure strata and its impact on water quality is of great significance to protect the groundwater environment in the tunnel area.

Relevant scholars have conducted a series of studies on water chemistry and water quality changes caused by tunnel construction. Li and Kagami [8] investigated the chemical composition and flow of groundwater from tunnel seepage and water from springs and wells around the tunnel and concluded that when tunnel seepage and diving and springs all come from the same aquifer, their chemical composition should be similar. Hasegawa et al. [9] established the relationship between the conductivity E and the location of the aquifer based on the changes of water chemistry and water quality in the fracture water at the tunnel palm face and effectively predicted the direction of the aquifer. Mossmark et al. [10, 11] monitored the water chemistry during the construction of the Harranza railroad tunnel, and the results showed that the groundwater infiltration into the tunnel changed the physicochemical properties of underground water, and the minerals underwent redox reactions, which releases SO_4^{2-}, and has a long-term influence on water chemistry. Based on the principal component analysis of groundwater samples from 31 tunnel boreholes, Saberinasr et al. [12] found that the main controlling factors of groundwater chemistry was water-rock interaction and the mineral dissolution process led to the excess concentration of many ions in water. Howladar and Rahman [13] conducted a comprehensive evaluation of granite mine tunnel wastewater quality, and the results showed that direct discharge of wastewater was hazardous to aquatic organisms.

Previous studies show that tunnel construction has great influence on the hydrogeochemical process and water quality of groundwater. However, less attention has been paid to the chemistry and quality of water in the gas-bearing coal stratigraphic section, especially the differences in the hydrochemical genesis of coal seam water and natural karst groundwater in the tunnel site area. At the same time, for karst tunnels, groundwater is abundant, and there is a huge potential for the use of groundwater discharged from the tunnels. The quality of groundwater mainly depends on the concentration of ions in the water, and water quality evaluation is the basis for deciding whether groundwater can be used. Therefore, it is very necessary to clarify the water-rock effect and groundwater quality of tunnel coal measure strata.

(a) (b) (c) (d)

Figure 3: Stratigraphic samples. (a) Coal seam on the tunnel face. (b) Coal seam. (c) Limestone intercalated with mudstone. (d) Mudstone.

In this paper, a case study based on the Tongzi Tunnel was conducted. Groundwater samples in the tunnel passing through the gas coal measure strata, in the side ditches of the main cave, and in the central drainage ditches of the main cave were collected to conduct laboratory experiments. Statistical methods were used to establish the connection between the tunnel and the hydrogeological environment and to evaluate the quality of coal measure formation water and surrounding karst groundwater. The main objectives of this study are as follows: (1) to describe the hydrochemical characteristics of coal seam water and karst water; (2) to analyze the evolution mechanism of groundwater chemistry in the tunnel through coal section and surrounding aquifers; and (3) to evaluate the suitability of coal seam water and discharged groundwater for drinking and irrigation and to analyze the main contaminant components and their sources. The results of the study can provide references for understanding the groundwater chemical characteristics in the tunnel through coal section and the utilization path of coal system water.

2. Tunnel Overview

2.1. Geographical Location. The tunnel is a typical superlong mountain highway tunnel, located in the northern Guizhou Plateau, the karst area of Southwest China. As shown in Figure 1, the tunnel starts at Dahe Town, through Tongzi County, and ends at Mazong Township, Tongzi County, with a total length of 10.5 km. The starting and stopping pile numbers of the left line are ZK34 + 508~ZK45 + 005, the elevation of the bottom plate at the inlet and outlet is 895.87 m and 1079.35 m, respectively, and the maximum buried depth is 649 m. The starting and stopping pile numbers of the right line are YK34 + 530~YK45 + 015, the elevation of the inlet and outlet floor is 896.30 m and 1079.25 m, respectively, and the maximum buried depth is 639 m. The longitudinal slope of the tunnel is 1.75%. The tunnel is dug at both ends of the entrance and exit to speed up construction, ventilation, and drainage; a total of four inclined shafts are set up. This study involves the groundwater of slant well No. 4.

Figure 4: Schematic diagram of sampling points.

Table 1: Sample points corresponding to pile numbers.

Group	Sample	Corresponding pile number	Group	Sample	Corresponding pile number
I	1	YK43+645	III	13	YK43+000
	2	YK43+715		14	YK43+150
	3	ZK43+800		15	YK43+350
	4	YK36+071.4		16	YK43+080
	5	YK43+140		17	YK43+200
	6	ZK43+287		18	YK43+610
	7	YK43+648		19	No. 4 inclined shaft
	8	YK43+650		20	No. 4 inclined shaft
	9	YK43+936		21	No. 4 inclined shaft
II	10	YK43+820	IV	22	No. 4 inclined shaft
	11	YK43+820		23	No. 4 inclined shaft
	12	YK43+930		24	No. 4 inclined shaft

2.2. Geology and Hydrogeology. The landforms in the tunnel site area are divided into two types: dissolution landforms and erosion landforms. The exposed bedrock mainly includes middle Permian Qixia formation (P_2q) limestone carbonaceous mudstone, middle Silurian Hanjiadian formation (S_1h) mudstone locally intercalated with argillaceous limestone, middle Silurian Shiniulan formation (S_1sh) argillaceous mudstone, middle Permian Maokou formation (P_2m) limestone, lower Triassic Maocaopu formation (T_1m) limestone, mudstone of the fifth member of the lower Triassic Yelang formation (T_1y^5) intercalated with marlstone, limestone of the fourth member (T_1y^4), mudstone of the third member (T_1y^3) intercalated with marlstone, limestone, argillaceous limestone, mudstone of the second member (T_1y^2), mudstone of the first member (T_1y^1), limestone of Changxing formation (P_3c) of upper Permian system, coal measure strata of upper Permian Longtan formation (P_3l), and lower Ordovician Meitan formation (O_1m) silty mudstone intercalated with limestone. In the exit section, the tunnel passes through Tuanyuanjie Coal Mine, Mazong

Table 2: Relative weights of groundwater quality parameters studied and reference standards.

Chemical parameter	WHO standards	Weight (w_i)	Relative weight (W_i)
pH	6.5-8.5	4	0.074
EC	1500	4	0.074
TDS	1000	4	0.074
HCO_3^-	500	3	0.056
SO_4^{2-}	250	5	0.093
Cl^-	250	4	0.074
NO_3^-	45	5	0.093
F^-	1.5	5	0.093
Ca^{2+}	75	2	0.037
Mg^{2+}	50	2	0.037
Na^+	200	3	0.056
K^+	12	2	0.037
NH_4^+	0.5	3	0.056
Fe	0.3	4	0.074
Al	0.2	4	0.074

Note: NH_4^+ and Al refer to WHO standards and Chinese groundwater quality standards [22, 23].

Table 3: Water quality classification.

Range	Type of water
<50	Excellent
50-100	Good
100-200	Poor
200-300	Very poor
>300	Unsuitable for any use

Table 4: Irrigation water quality evaluation index.

Parameters	Formula
SAR	$\frac{Na^+}{\sqrt{(Ca^{2+}+Mg^{2+})/2}}$
Na^+%	$\frac{Na^+ + K^+}{Na^+ + K^+ + Ca^{2+} + Mg^{2+}} * 100$
RSC	$\left(HCO_3^- + CO_3^{2-}\right) - \left(Ca^{2+} + Mg^{2+}\right)$
PS	$Cl^- + 0.5SO_4^{2-}$
PI	$\frac{\left(Na^+ + \sqrt{(HCO_3^-)}\right)}{Na^+ + Ca^{2+} + Mg^{2+}} * 100$
MH	$\frac{Mg^{2+}}{Ca^{2+} + Mg^{2+}} * 100$
KI	$\frac{Na^+}{Ca^{2+} + Mg^{2+}}$
TH	$Ca^{2+} + Mg^{2+}$

Township, Tongzi County; the coal mine transportation lane is about 79 meters away from the roof of the tunnel; coal mine goaf is more sensitive to tunnel construction response. The geological longitudinal section of the tunnel is shown in Figure 2.

The Songkan River, Tongzhi River, and Qingxi River in the area are all mountainous rain-fed rivers, which are mainly recharged by precipitation runoff.

Under the influence of stratum lithology, the groundwater in the tunnel field is widely recharged by meteoric water and some surface water and infiltrates through the fissure dissolver, and the groundwater is basically the infiltration runoff type. The rainy period is from June to August; after December, the rainfall is significantly reduced. The buried depth of groundwater is generally 50~100 m and larger than 200 m in some sections; the tunnels are basically located below the groundwater level.

2.3. Coal Seams and Gas. The P_3l coal seam in the tunnel site area contains 7 layers of coal (lines), which can be numbered from C1 to C7 from bottom to top, and there are three recoverable coal seams (C3, C5, and C6). The coal seam is black, gray-black semidark to semibright bituminous, with asphalt luster and a small amount of glass luster; the coal seam dip angle at the tunnel through the coal about 70° is sharply inclined coal seam, coal rock structure damage type III (strongly damaged coal). The lithological combination of this set of coal system strata is complex, and the lithology includes carbonaceous mudstone, siltstone, and sandstone with several thin layers of tuff, mudstone, marl, carbonaceous tuff, flint limestone, and coal seam, with brownish gray and grayish white aluminous mudstone at the bottom and contains more sulphide iron ore. The rock samples are shown in Figure 3.

Tongzi Tunnel has high gas content and high gas pressure in the coal-penetrating section, and the grade of gas section is class 1. According to the data measured in the Liangfengya Tunnel, which is similar to the Tongzi Tunnel and crosses the same coal seam, the absolute gush of CH_4 from the new Liangfengya Tunnel P_3l coal seam is 1.37 m^3/min~7.17 m^3/min and the absolute gush of CO_2 is 0.54 m^3/min~2.81 m^3/min, with a maximum gas pressure of 1.5 MPa.

2.4. Climate. The average annual temperature in the tunnel area is 14.7°C, with an extreme maximum of 36.6°C and an extreme minimum of -6.9°C. The average annual precipitation is 1037.3 mm, the maximum annual rainfall is 1374 mm, the maximum daily rainfall is 137.3 mm, and the average annual evaporation is 1119.5 mm.

3. Materials and Methods

3.1. Sample Collection and Analysis. According to the actual construction progress and research purpose of the tunnel, a total of four sets of samples were collected. Among them, group I is the groundwater samples from the tunnel main cavern seepage, mainly concentrated in the coal-bearing stratigraphic section; group I can approximately represent the groundwater in the original coal-bearing aquifer. Group

Table 5: Statistics of groundwater water chemical parameters (mg/L).

	Group I			Group II			Group III			Group IV		
	Mean	Min	Max	Mean	Min	Max	Mean	Min	Max	Mean	Min	Max
pH	8.32	7.98	8.61	8.45	8.27	8.60	8.69	8.56	8.95	8.38	8.08	8.62
EC	332.38	138.00	601.00	254.25	188.00	328.00	299.33	211.00	516.00	229.67	31.00	282.00
TDS	165.88	69.00	300.00	126.50	94.00	163.00	148.67	106.00	253.00	114.50	16.00	140.00
HCO_3^-	117.95	0.00	190.69	101.28	3.43	183.06	75.64	0.00	179.25	107.53	19.07	163.99
SO_4^{2-}	53.90	0.42	122.56	37.50	8.29	69.41	83.53	70.27	114.79	26.23	5.77	53.78
Cl^-	1.32	0.35	2.76	1.51	0.69	1.94	1.70	1.43	2.20	0.91	0.18	1.82
NO_3^-	6.26	1.15	30.20	3.50	0.28	6.67	4.33	3.00	5.26	2.84	0.68	5.07
F^-	0.41	0.22	0.74	0.65	0.24	1.53	0.47	0.20	0.60	0.21	0.11	0.33
Ca^{2+}	34.31	1.56	69.31	21.64	0.00	46.81	28.32	2.90	64.27	38.12	0.19	57.55
Mg^{2+}	22.18	0.00	69.20	5.21	3.36	7.07	3.55	0.00	5.82	8.89	0.00	23.86
Na^+	18.58	1.15	40.20	27.62	6.55	38.74	25.12	14.80	32.59	6.53	0.23	11.69
K^+	8.29	0.82	45.42	11.10	2.02	29.72	18.98	4.34	47.66	3.34	0.13	7.20
NH_4^+	1.04	0.00	6.63	0.16	0.00	0.48	0.04	0.00	0.22	0.06	0.00	0.24
Fe	0.36	0.00	0.78	0.23	0.00	0.59	0.32	0.08	0.74	0.28	0.00	0.53
Al	0.03	0.00	0.11	0.07	0.00	0.23	0.17	0.02	0.76	0.03	0.00	0.08

Note: pH is dimensionless, conductivity unit is s-cm^{-1}, and other units are mg/L.

II is the groundwater samples in the central drainage ditch, mainly from YK43+820 to the direction of large mileage. Group III is the groundwater samples in the side trenches of the main tunnel, mainly concentrated under the coal measure stratum. Due to the slope of the tunnel, the coal measure stratum water may flow into the side trenches through seepage. Group IV is groundwater samples from slanting well No. 4 without coal strata, which can be used as the observation group for comparative analysis. The water intake point is shown schematically in Figure 4, and the corresponding tunnel cross-section stakes are shown in Table 1.

Before sampling, raw water was used to wash the bottle, and the cap was tightened in the water to prevent the air from entering. The water sample was drip-fed with nitric acid until pH < 2. The water samples used for testing cations were titrated with nitric acid to pH < 2. The anions F^-, Cl^-, SO_4^{2-}, and NO_3^- were determined by ion chromatography, and HCO_3^- was titrated by acid-base titration. Cations K^+, Ca^{2+}, Na^+, and Mg^{2+} were determined by flame atomic absorption spectrophotometry. All the above tests were carried out in the College of Resources and Environmental Engineering and the Key Laboratory of Karst Environment and Geological Hazards, Guizhou University.

3.2. Research Methodology

3.2.1. Integrated Approach to Water Chemistry. Groundwater chemistry is the result of the interaction between the groundwater and the rocks and minerals of the aquifer. To study the main processes of hydrochemical evolution of groundwater, experimental data were plotted on piper diagrams and Gibbs plots to visually analyze the relative content and hydrochemical characteristics of conventional ions in groundwater [14, 15]; the main causes of ions in groundwater were revealed by scatter plots and correlation analysis, the correlation coefficient r ranges from -1 to 1, and larger value indicates a stronger correlation between the chemical parameters [16]. The saturation index (SI) of the main minerals in the study area was calculated using the PHREEQC software, and the aqueous solution was saturated when the SI was greater than 0. When the SI was less than 0, the minerals continued to dissolve [17].

3.2.2. Water Quality Assessment

(1) WQI Water Quality Index. Water quality index is a comprehensive value calculated by the experimental results of several parameters to analyze the water quality status visually and quantitatively. The calculation process is divided into the following four steps [18–21]:

Step 1. The relative weight W_i is calculated based on the weight ω_i of each indicator, and the calculation formula is shown in

$$W_i = \frac{\omega_i}{\sum_{i=1}^{n} \omega_i}, \tag{1}$$

where ω_i is the weight of the indicator; the weights of each indicator are shown in Table 2; W_i is the relative weight; and n is the number of indicators.

Step 2. The quality evaluation index q_i is calculated based on

$$q_i = \frac{c_i}{s_i} \times 100, \tag{2}$$

where c_i is the measured concentration of each indicator; s_i is the World Health Organization (WHO) standard value

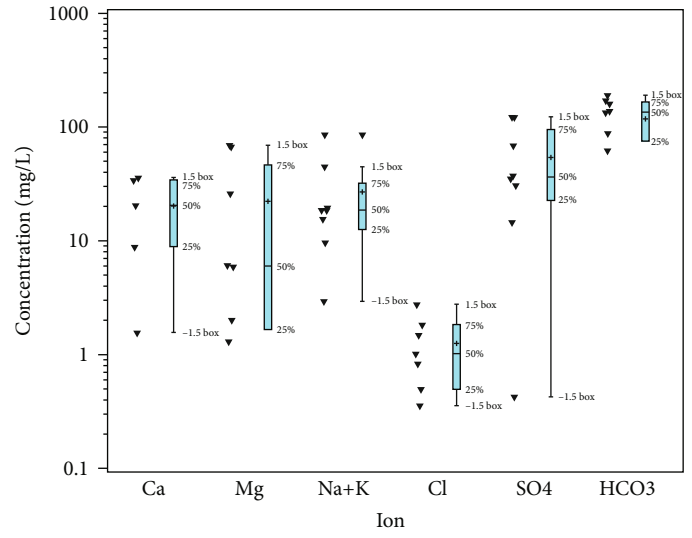

(a)

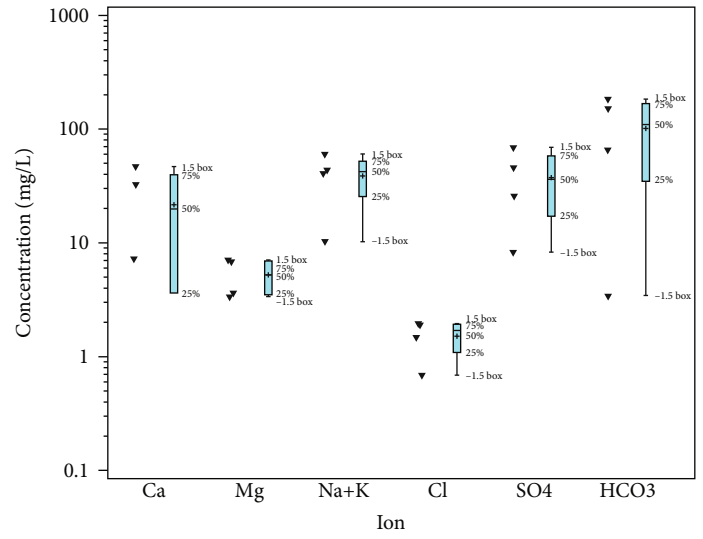

(b)

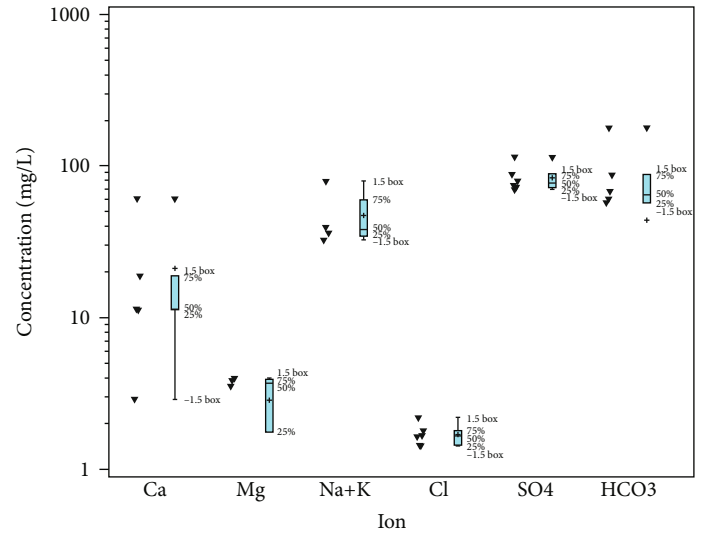

(c)

Figure 5: Continued.

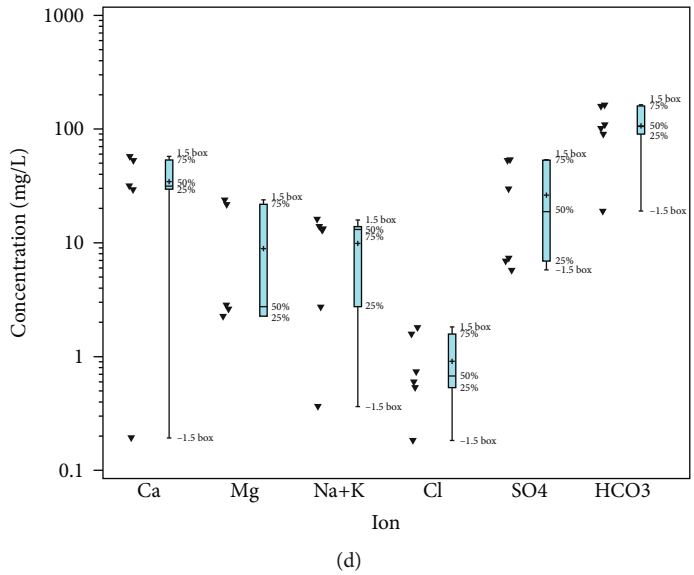

(d)

Figure 5: Major ion box diagram of the study area.

corresponding to the indicator; and q_i is the quality evaluation index.

Step 3. The subindex SI_i for each sample is calculated based on Equation (2).

$$SI_i = W_i \times q_i. \tag{3}$$

Step 4. The water quality index WQI is calculated for each sample based on Equation (4), and the water quality condition is judged according to the WQI value and the rating criteria in Table 3.

$$\mathrm{WQI} = \sum_{i=1}^{n} SI_i. \tag{4}$$

(2) Irrigation Water Quality Assessment. The chemical composition of irrigation water affects plant metabolism and soil permeability [24], and indicators commonly used to evaluate the suitability of irrigation water are sodium sorption rate (SAR), sodium percentage (Na^+%), residual sodium carbonate (RSC), potential salinity (PS), permeability index (PI), magnesium hazard (MH), Kelly index (KI), and total hardness (TH) [18, 25]. The formulae for these indicators are shown in Table 4, and the ion concentrations in the formulae are in meq/L.

4. Results and Discussion

4.1. Water Chemical Composition Concentration. The statistics of the concentration of each ion in the water samples are shown in Table 5, and the main ion box plots are shown in Figure 5. The results show that the overall water samples in the study area are weakly alkaline, with the maximum mean pH value of 8.69 in group III and the minimum mean pH value of 8.32 in group I. The maximum mean TDS value of 165.88 in group I and the minimum mean TDS value of 114.50 in group IV indicate that the tunnel coal seam water is subjected to the longest water-rock action and has the most inorganic salts and dissolved substances. The inorganic salts and dissolved substances in the water are the most abundant. The trend of conductivity is basically the same as TDS. The overall anions in the study area show HCO_3^-> SO_4^{2-}> Cl^-, and Na^++K^+ is higher in the cations compared to the carbonate strata due to the presence of coal strata [26].

4.2. Water Chemistry Types and Water Chemistry Characteristics

4.2.1. Water Chemistry Type. The Piper diagram of the study area is shown in Figure 6. It can be seen that group I cations are more dispersed in the diagram, while anions are basically distributed in the HCO_3^- line side. In the diamond diagram of the Piper diagram, the water sample points basically fall in zone 1, and the groundwater type is mainly Ca-HCO_3 type. Group II cations are near the Na^++K^+ end, and anions are scattered on the side of HCO_3^- and SO_4^{2-}. In the diamond shape of the Piper diagram, the water sample points fall in zones 1, 2, and 5, and there are more groundwater types, including Ca-HCO_3 type, Na-Cl type, and mixed type. Group III cations are obviously concentrated at the Na^++K^+ end, while the anions are distributed on the SO_4^{2-} side of the line. In the diamond-shaped plot of the Piper diagram, the water sample points mainly fall in zone 2, and the groundwater type is mainly Na-Cl type, followed by Ca-HCO_3 type. Group IV cations are scattered at the Ca^{2+} and Mg^{2+} end, and anions are concentrated on the HCO_3^- side of the line. In the diamond shape of the Piper diagram, the water sample points all fall in zone 1, and the groundwater types are all of Ca-HCO_3 type.

From this, it can be tentatively judged that the water chemistry components of karst groundwater in the study area are mainly controlled by the water-rock action of

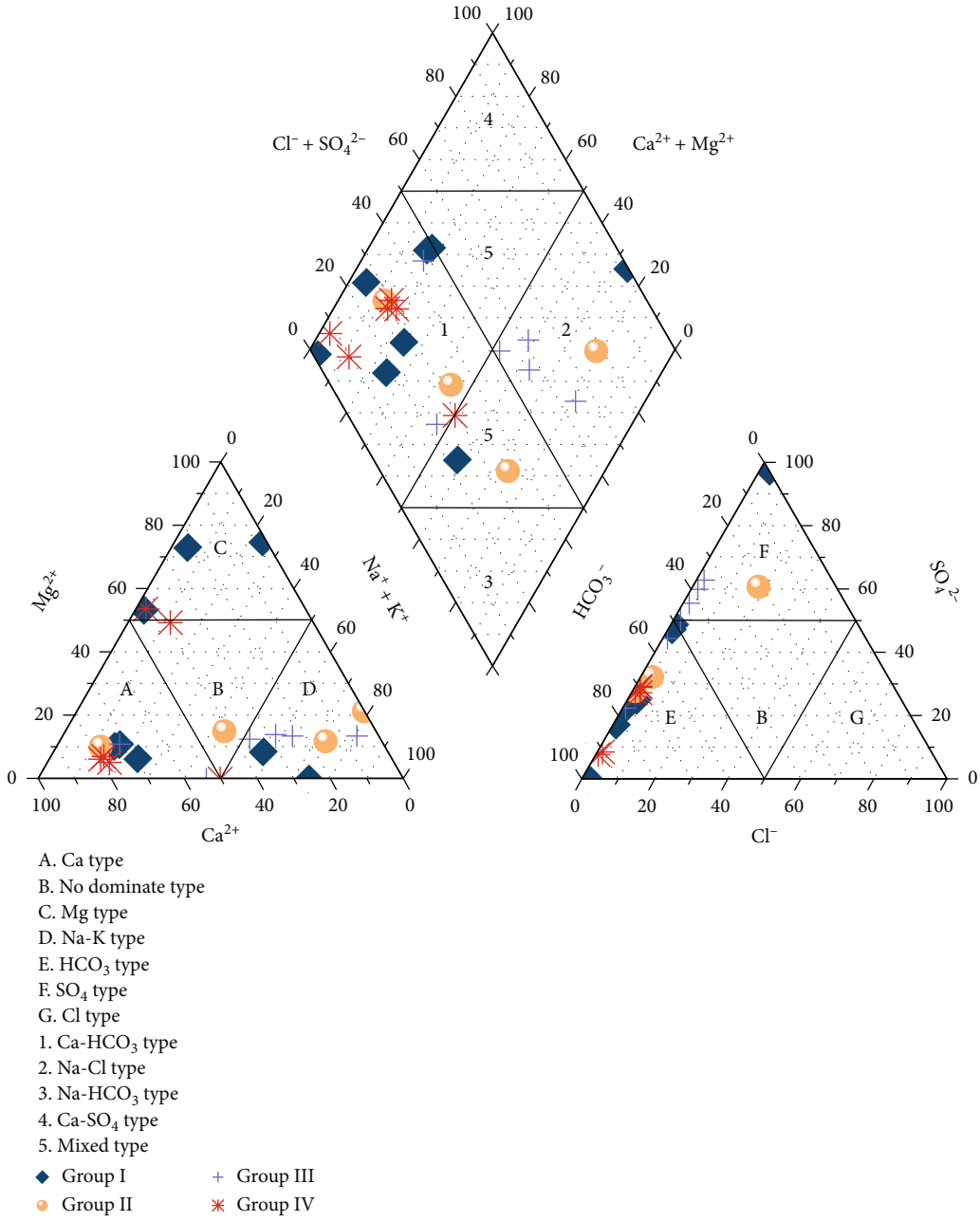

Figure 6: Piper diagram of the chemical composition of water in the study area.

carbonate rocks and other minerals. The distribution of group I samples is more scattered in the map without obvious patterns. This indicates that compared with the groundwater in the drainage ditch, the water chemistry of coal system water is more directly affected by the lithology of the strata, and the lithology of the strata in different water extraction sections is different; also, the water-rock action is more complicated when the surrounding rock alternates with the coal strata. The groundwater collected in the side ditches and central drainage ditches of the main cave may pass through more rock formations due to the long runoff paths, and from a wider range of sources, but the lithology may not be as complex as that of group I. In general, the hydrochemical types are still different. Since the stratigraphic lithology of No. 4 slanting well is single, the cave surrounding rocks are mainly medium weathered tuff and medium weathered surrounding rocks interspersed with carbonaceous mudstone, so the distribution of the IV water sample points is concentrated and the water chemistry type is single.

4.2.2. Mechanisms Controlling the Evolution of Water Chemistry. In the Gibbs model, the logarithm of mass concentration of TDS is set as the ordinate, and the cation ratio $Na^+/(Na^+ + Ca^{2+})$ or anion ratio $Cl^-/(Cl^- + HCO_3^-)$ is set as the abscissa; thus, the three natural control factors of the main ions in the water, including evaporation and concentration control, water-rock interaction control, and

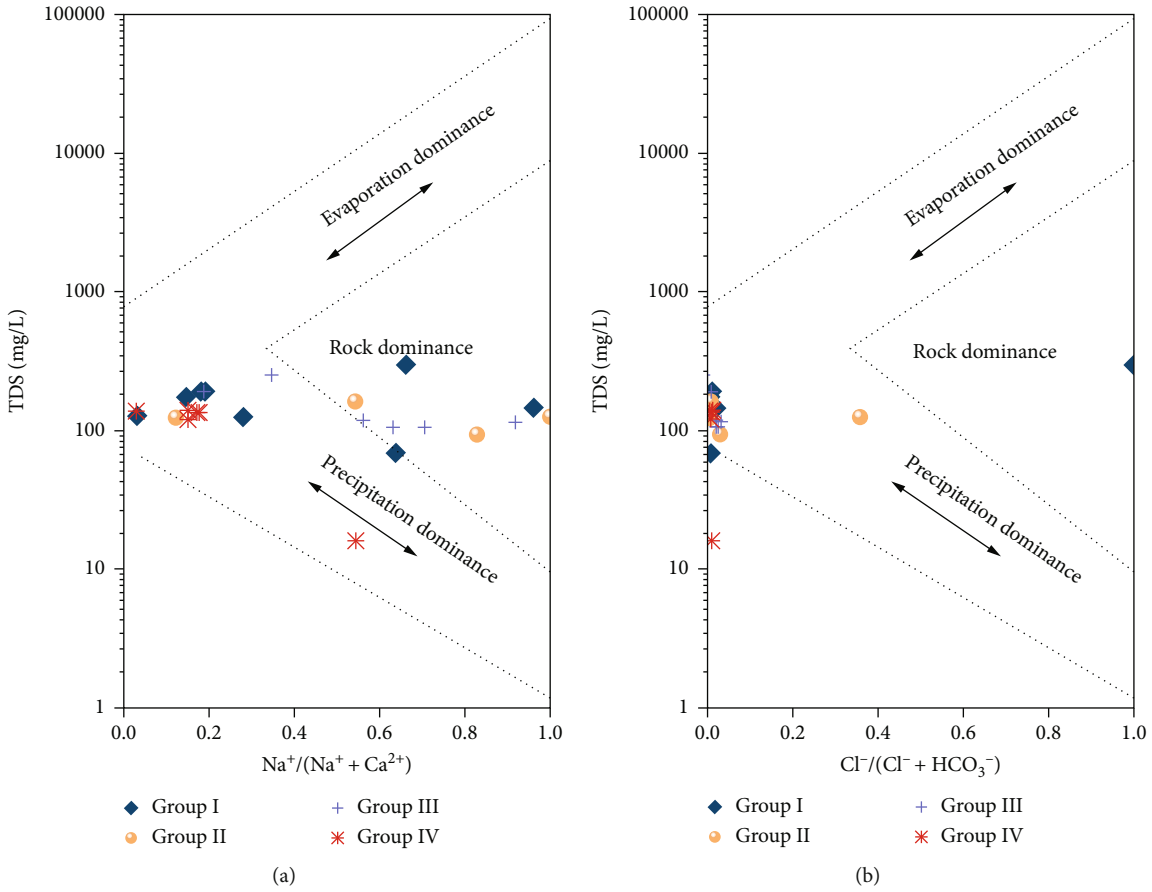

Figure 7: Gibbs plot of groundwater samples in the study area.

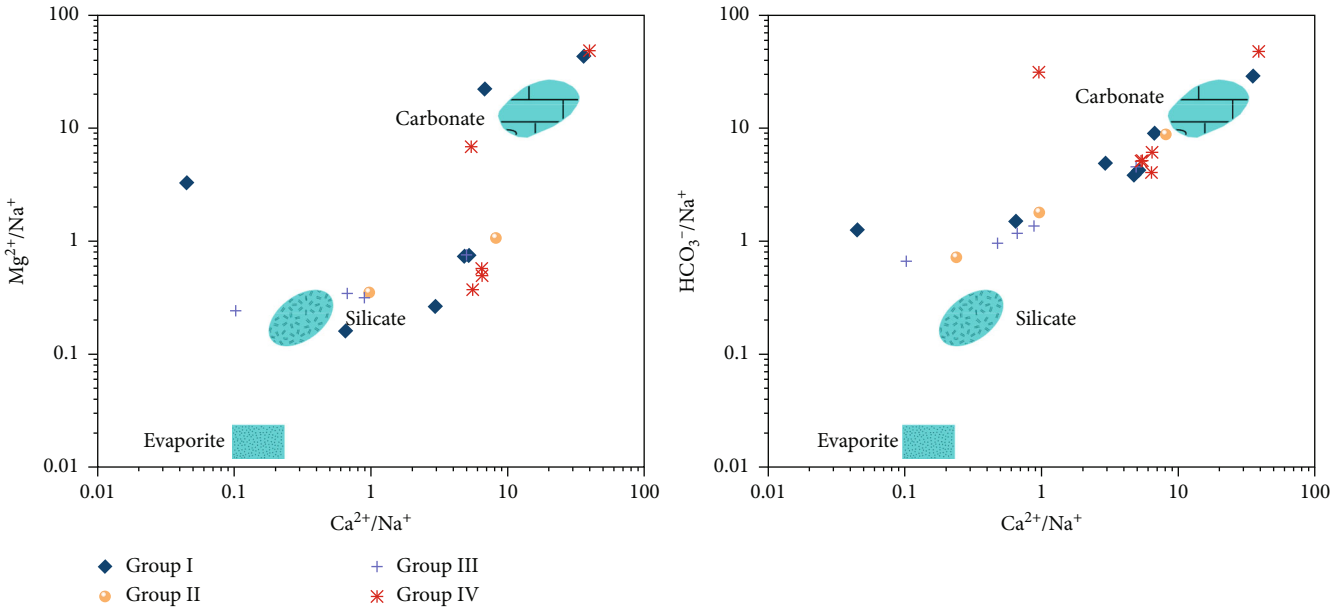

Figure 8: The ratio of Mg^{2+}/Na^{+} to Ca^{2+}/Na^{+} and HCO_3^{-}/Na^{+} to Ca^{2+}/Na^{+}.

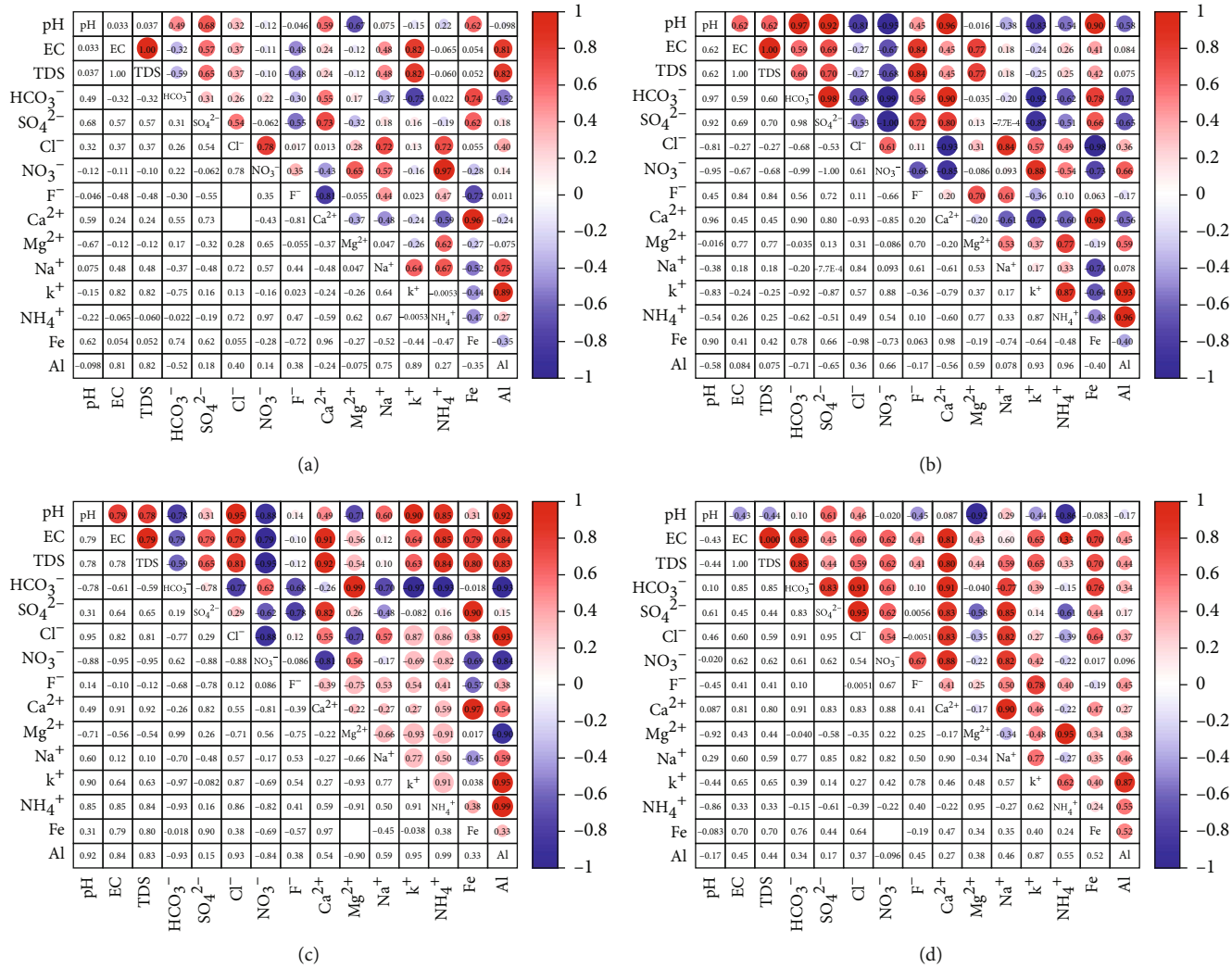

Figure 9: Correlation matrix of ions in groundwater in the study area.

atmospheric precipitation, can be macroscopically reflected [27]. As shown in Figure 7, it can be seen that the groundwater samples are basically located in the middle of the Gibbs diagram, spanning the entire range (0.1~0.9) of $Na^+/(Na^+ + Ca^{2+})$ values. This may indicate that the water chemical composition of the study area is mainly controlled by water-rock action, and atmospheric precipitation has some influence on individual points, but evaporation and crystallization are not obvious.

The position of groundwater on the left or right side of the diagram depends on the groundwater runoff path. The $Na^+/(Na^+ + Ca^{2+})$ ratio decreases when carbonate minerals dominate and may be higher when silicate minerals dominate [28]. The end element comparison between different lithologies can determine the effect of weathering dissolution of different rocks on the groundwater solute. Figure 8 shows that the groundwater samples are basically located between the carbonate and silicate control end elements. The group II water samples are close to the silicate rock control end, and the group III water samples are closer to the carbonate rock control end.

4.3. Water-Rock Action

4.3.1. Correlation Analysis. To maintain equilibrium in groundwater solutions, such as anions and cations and dissolved precipitation, there must be correlations between the ions, and correlation analysis can determine whether the ions are homologous [29]. As can be seen in Figure 9, TDS is highly correlated with K^+ and Al, and the correlations of HCO_3^--Ca^{2+} and Ca^{2+}-Mg^{2+} are lower, which may be related to the complex mineralogical composition of the coal-bearing strata. This indicates that besides carbonate rocks, mineral dissolution such as alunite and hydrargyrite also has an important contribution to the ions in group I water. In group II water samples, the correlations of HCO_3^--SO_4^{2-}, HCO_3^--Ca^{2+}, SO_4^{2-}-Ca^{2+}, and Cl^--Na^+ are high, indicating that these ions are of consistent origin and conventional carbonate rock, silicate rock, and gypsum dissolution are the main ionic genesis in the central drainage. The SO_4^{2-}-Ca^{2+} and HCO_3^--Mg^{2+} correlations in group III water samples are high, while the HCO_3^--Ca^{2+} correlation is low, indicating that the contribution of dolomite to Ca^{2+}

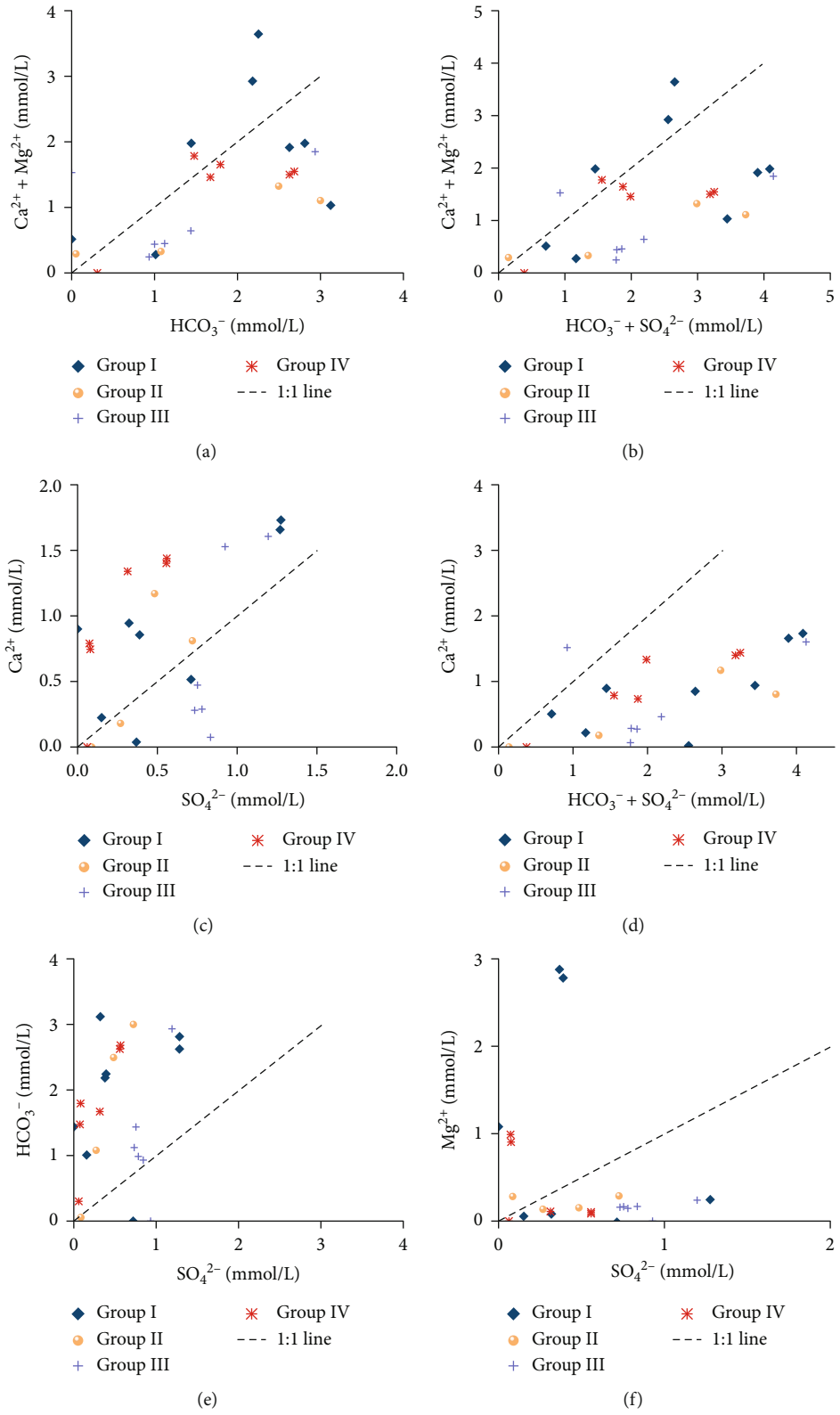

Figure 10: Continued.

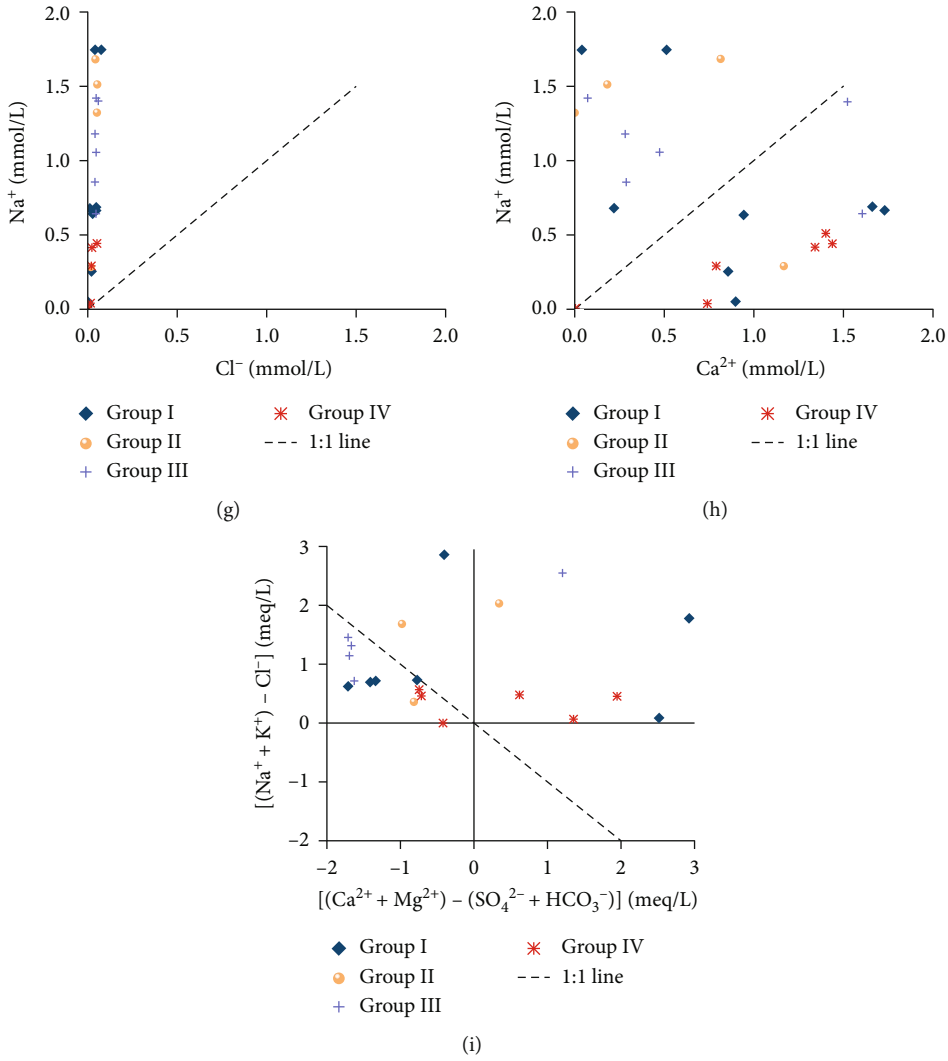

Figure 10: The relationship between the main ion ratios in the tunnel area.

is greater than that of calcite, and Ca^{2+} may come from gypsum in addition to carbonate rocks. The water samples of group IV showed high correlation between HCO_3^--Ca^{2+}, SO_4^{2-}-Ca^{2+}, and Cl^--Na^+, indicating that the sources of these ions may be consistent, mainly for carbonate rocks, sulfate, and salt rocks.

4.3.2. Major Ion Ratio Relationship. Figure 10 shows the main ion relationships in each group of samples, and Ca^{2+}, Mg^{2+}, and HCO_3^- in groundwater and surface water in the karst area are mainly from dissolved carbonate rocks [30], and the products of carbonate rock dissolution should satisfy that $\gamma(Ca^{2+}+Mg^{2+})/\gamma HCO_3^-$ equals to 1. As shown in Figure 10(a), most of the water samples fall below the 1 : 1 equivalence line; combined with Figure 10(b) in addition to the dissolution of carbonate, there is also the dissolution of sulfate minerals.

If all SO_4^{2-} in groundwater in the tunnel area is derived from the dissolution of gypsum, the Ca^{2+} has a good linear relationship with SO_4^{2-}, and $\gamma Ca^{2+}/\gamma SO_4^{2-}$ should be 1 : 1. From the amount ratio relationship between Ca^{2+} and SO_4^{2-} in Figure 10(c), it can be seen that the water samples in group II are mainly distributed on the 1 : 1 contour, which indicates that the SO_4^{2-} in this group of water samples mainly comes from the dissolution of gypsum. For most of the water samples in group III, the $\gamma Ca^{2+}/\gamma SO_4^{2-}$ is below the 1 : 1 contour. Overall, the contribution of gypsum to Ca^{2+} in group III water samples is greater than that of carbonate rocks. As shown in Figure 10(e), $\gamma HCO_3^-/\gamma SO_4^{2-}$ is near the 1 : 1 contour, indicating that the carbonate rocks in group III are mainly dolomite dissolved, and the high correlation between Mg^{2+} and HCO_3^- confirms this inference. The $\gamma Ca^{2+}/\gamma SO_4^{2-}$ values in group IV water samples are all distributed on the upper side of the 1 : 1 line with good correlation, which also proves that the gypsum is one of the sources of Ca^{2+} and SO_4^{2-}, and there is also excess Ca^{2+}, which has high correlation with HCO_3^-. It is believed that the calcite in carbonate rocks have an important contribution to Ca^{2+} in group IV water samples.

The coal seam water samples are more dispersed in Figure 10, and there is no obvious linear relationship between ions, while the correlation of Ca^{2+}, Mg^{2+}, HCO_3^-,

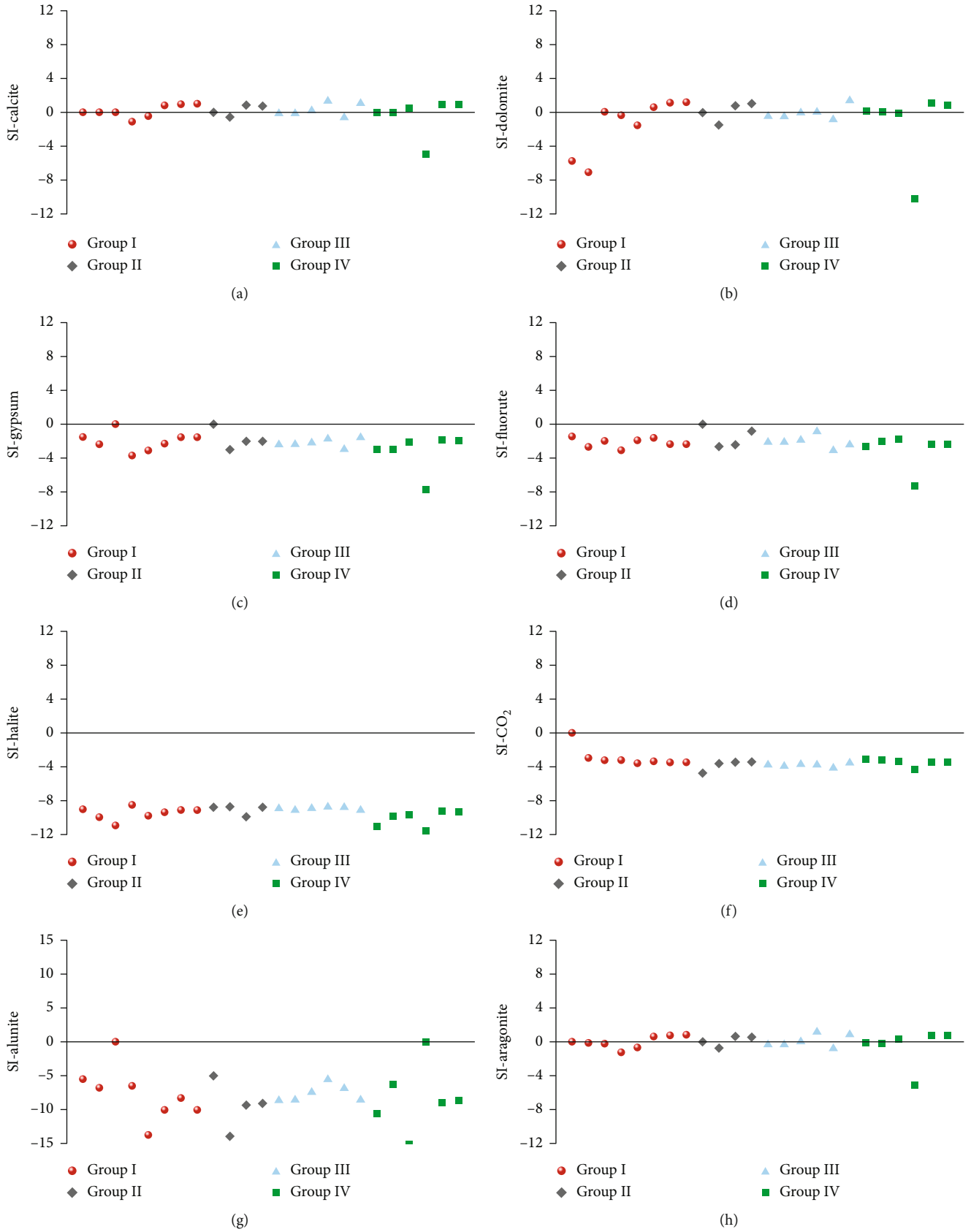

Figure 11: Continued.

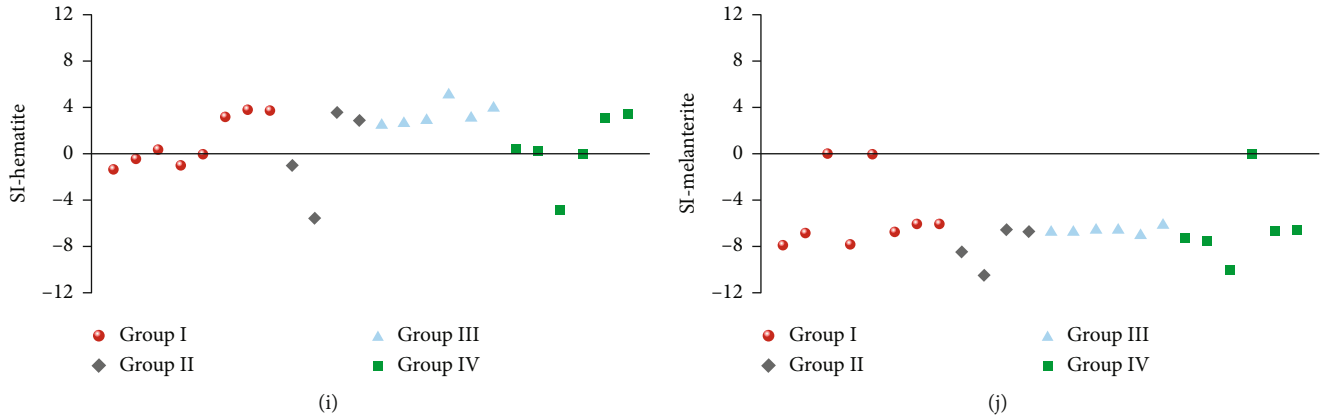

Figure 11: Saturation index of major minerals in the study area.

Table 6: Water quality classification results based on water quality indices.

Group	Sample	WQI	Water quality	Group	Sample	WQI	Water quality
I	1	47.18	Excellent	III	13	27.50	Excellent
	2	33.15	Excellent		14	27.70	Excellent
	3	29.65	Excellent		15	31.14	Excellent
	4	107.54	Poor		16	81.90	Good
	5	18.65	Excellent		17	33.48	Excellent
	6	38.24	Excellent		18	44.45	Excellent
	7	45.43	Excellent		19	27.45	Excellent
	8	44.48	Excellent		20	32.62	Excellent
	9	38.65	Excellent		21	18.98	Excellent
II	10	18.45	Excellent	IV	22	9.09	Excellent
	11	34.56	Excellent		23	31.08	Excellent
	12	39.05	Excellent		24	34.67	Excellent

and SO_4^{2-} is also low. It shows that the water samples in this group are obviously influenced by lithological differences, and the Ca^{2+}, Mg^{2+}, HCO_3^-, and SO_4^{2-} ions among individual groundwater samples are not uniform in genesis and generally controlled by carbonate, sulfate, and silicate rocks.

If the Na^+ in the study area originates from salt rock dissolution, the molar ratio of $\gamma Na^+/\gamma Cl^-$ should be 1 : 1 [31]. According to Figure 10(g), the $\gamma Na^+/\gamma Cl^-$ values of all samples are far above the 1 : 1 contour. Except for group III, the correlation between Na^+ and Cl^- in other water samples is good. This suggests that a small amount of rock salt dissolution exists in groundwater, but rock salt dissolution is not the only cause controlling the Na^+ content, and there may be other causal mechanisms for Na^+ in groundwater, such as silicate weathering dissolution in nature, mannite dissolution, and other water-rock effects.

The relationship between $\gamma[(Na^+ + K^+) - Cl^-]/\gamma[(Ca^{2+} + Mg^{2+}) - (HCO_3^- + SO_4^{2-})]$ and $\gamma Na^+/\gamma Ca^{2+}$ allows the analysis of ion exchange in groundwater chemistry and characterization of the degree of mineralization during groundwater evolution [32]. Usually, the main cation exchange in groundwater is Ca^{2+}-Na^+ ion exchange, and the process is reversible. As can be seen from Figure 10(i), the $\gamma[(Na^+ + K^+) - Cl^-]/\gamma(Ca^{2+} + Mg^{2+}) - (HCO_3^- + SO_4^{2-})$ of most of the water samples in group III and group I has negatively linear correlation. This reflects the adsorption of Ca^{2+} and the release of Na^+, which are closely related to the silicate rock minerals and clay minerals in the surrounding rocks. The small $\gamma Na^+/\gamma Ca^{2+}$ ratio of all water samples in group IV indicates that the Ca^{2+} concentration is greater than Na^+ in these water samples, at which time the Ca^{2+} in groundwater exchanges for Na^+ adsorbed on the surface of solid particles.

4.3.3. Analysis of Mineral Saturation Index Results. The dynamic equilibrium of groundwater mineral phase is the result of water-rock interaction, and the reaction state between groundwater, surrounding rock, and minerals can be judged according to the saturation index SI. As shown in Figures 11(a) and 11(b), calcite dissolution was in equilibrium in most of the water samples, and dolomite dissolution continued to dissolve in some of the water samples in group I without reaching equilibrium, indicating that nonequal dissolution of two minerals occurred in the coal-bed water. The CO_2 saturation index of the coal aquifer is larger than that of other aquifers, which shows that the high pH of coal bed water slows down the dissolution rate of CO_2.

As shown in Figures 11(c)–11(g) and 11(j), the saturation indices of gypsum, fluorite, saltpeter, carbon dioxide, alum, and water green alum in the study area are less than

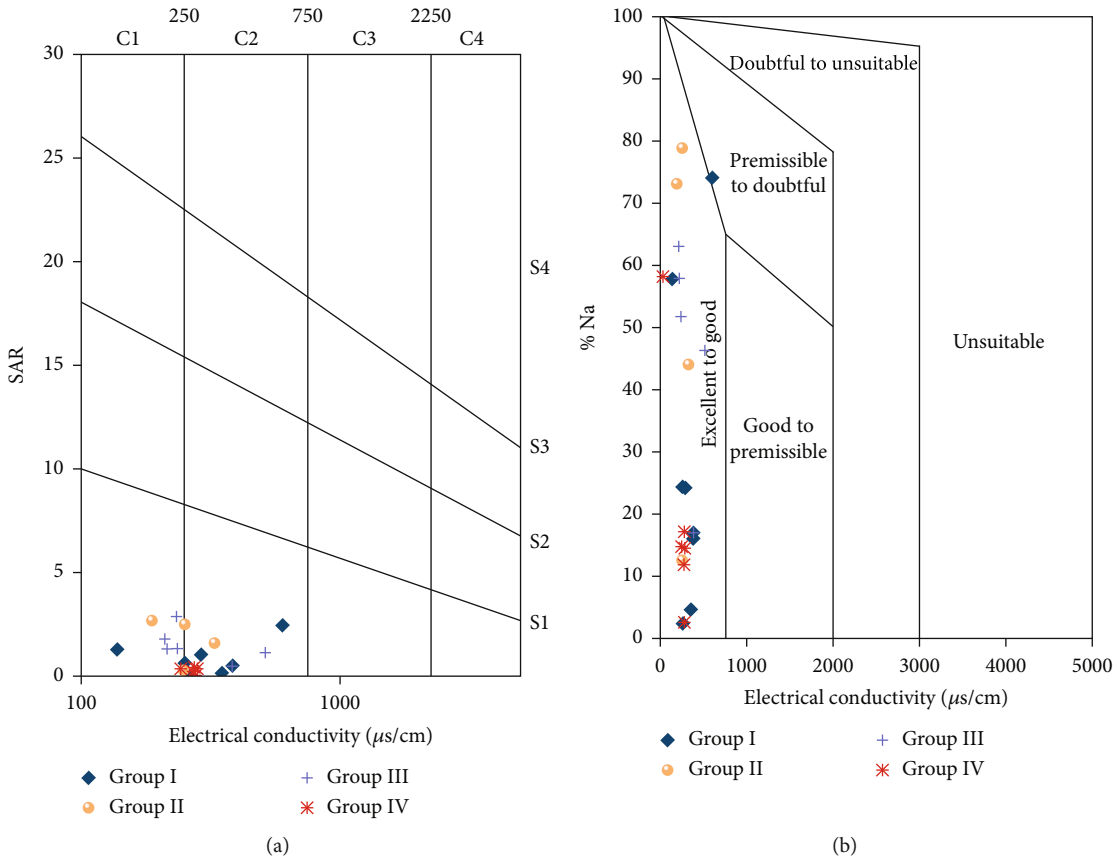

Figure 12: USSL and Wilcox plots for tunnel irrigation water classification.

0, indicating that these minerals are in a dissolved state and none of them have reached saturation, and the participation of these minerals in aqueous rock action is the main cause of Ca^{2+}, Mg^{2+}, F^-, Na^+, Cl^-, Al, and Fe in groundwater. Figures 11(h)–11(i) show that the dissolution of aragonite and hematite in the study area has basically reached saturation, except for a few sampling points.

4.4. Water Quality Evaluation

4.4.1. Analysis of WQI Calculation Results. The results of WQI water quality index calculation are shown in Table 6. The mean value of WQI was 45.54 of water samples in group I, 32.68 of group II, 41.03 of group III, and 25.65 of group IV. Sample 4 of group I has the highest WQI value, with the sampling point at section YK36+071.4, where the surrounding rocks of the cave are medium-weathering tuff, muddy tuff with marl, and muddy siltstone.

Excluding the 4th sample, the mean value of WQI of water samples in group I is still higher than those in groups II and IV. Although the groundwater in the central drainage ditch and side ditches of the tunnel main cavern was exposed to air, the water quality did not deteriorate significantly. The best groundwater quality is found in the side trench of No. 4 slant shaft. Overall, the water quality is good, with 91.6% of high-quality water. The water quality is mainly affected by the special stratum; also, the reaction between groundwater and minerals after the tunnel construction exposes minerals, which results in high metal ion concentration in the water and affects the water quality.

4.4.2. Analysis of Irrigation Water Quality Results. The USSL plot method (Figure 12(a)) and the Wilcox plot method (Figure 12(b)) are two commonly used methods to reflect the quality of irrigation water. As can be seen from Figure 12(a), all four groups of water samples fall in the range of C1-S1 and C2-S1, indicating that the study area is mainly a low-sodium medium saline water body.

As shown in Figure 13, the PI value shows that one coal seam groundwater is in the "unsuitable" condition, the MH value indicates that 29.16% of the water samples are in the "unsuitable" condition, and the KI value indicates that 25% of the water samples are in the "unsuitable" condition. The RSC, TH, and PS values of all water samples are within the "suitable" range.

It indicates that higher concentrations of Mg^{2+} and Na^+ in some water samples are the main factors leading to unsuitable water quality for irrigation and that high concentrations of Mg reduce soil permeability. Most of the water samples unsuitable for irrigation come from the coal stratigraphic section, reaching 62.5%, followed by groundwater in the No. 4 inclined shaft and the central drainage ditch. According to the previous analysis, the higher Mg^{2+} and Na^+ in these water samples mainly originates from clay minerals and ion exchange.

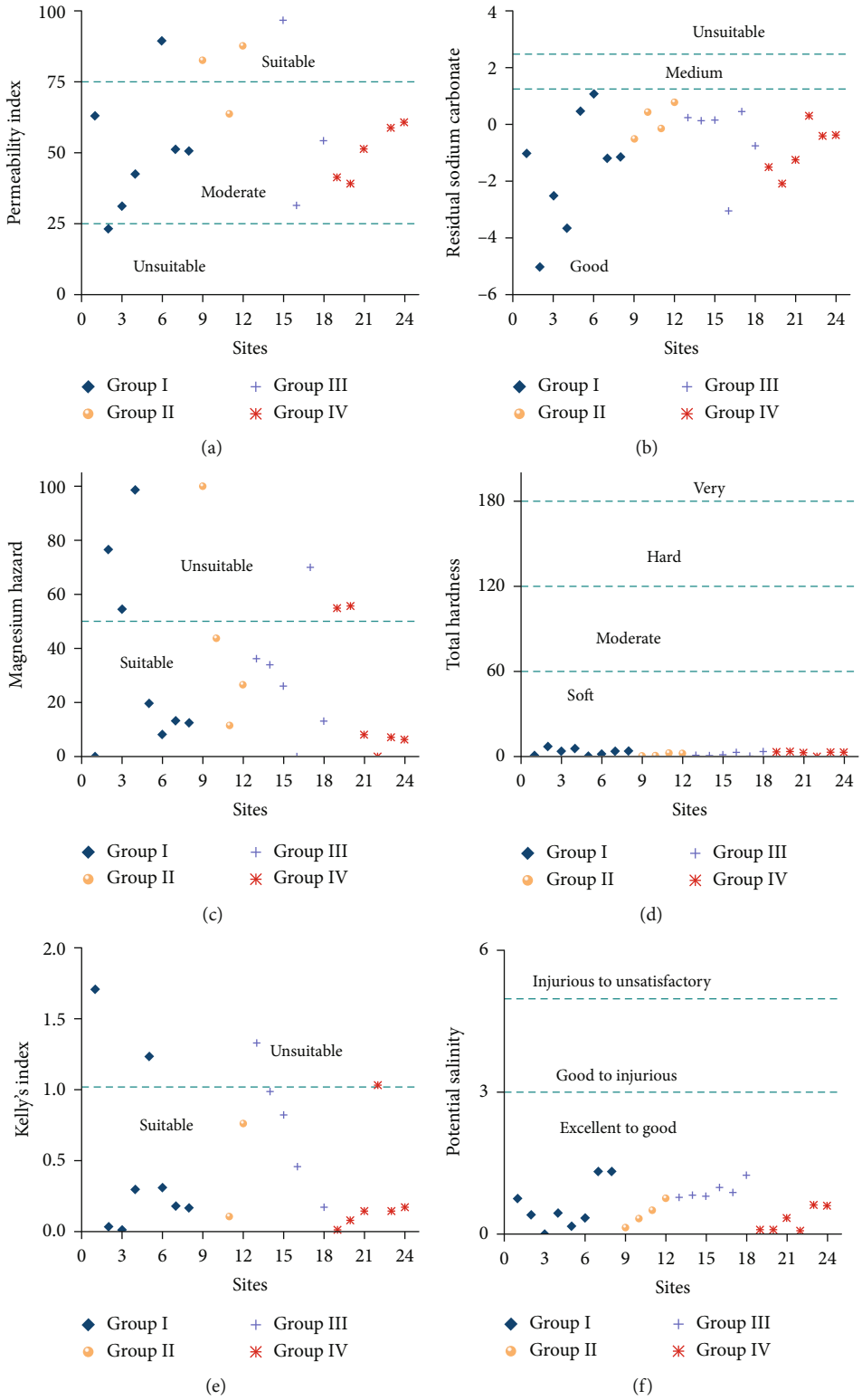

Figure 13: Irrigation water quality-related index.

5. Conclusion

In this study, the evolution of groundwater in the coal-bearing section of the Tongzi Tunnel, and other sources was analyzed by various methods, and the potability and irrigability of the discharged groundwater were evaluated. Based on these studies, the following conclusions were drawn.

(1) The water-rock interaction between groundwater and minerals in coal strata during runoff is the main cause of coal strata water. The main control mechanisms of water chemistry are dissolution and precipitation of minerals, oxidation and reduction, ion exchange and ion adsorption, and desorption. Compared with the drainage path and runoff time, the complex chemical reactions in the coal seam have a significant impact on the hydrological properties of groundwater in the coal seam, and the major ions in groundwater in the original aquifer show better correlation and more homogeneity due to the single lithology

(2) The main sources of Ca^{2+}, Mg^{2+}, and HCO_3^- in the study area are dissolved carbonate rocks and silicate rocks, among which the dissolved carbonate rocks in the groundwater of group III are mainly dolomite, and Ca^{2+} in the groundwater of group IV is mainly from calcite. SO_4^{2-} in karst aquifers is mainly derived from gypsum dissolution, and excess SO_4^{2-} in coal strata is also mainly derived from sulphide iron ore. Cl^- is relatively stable and derived from the dissolution of rock salt. In addition to salt rock dissolution, the major source Na^+ comes from silicate and cation exchange

(3) According to the results of mineral saturation index calculation, gypsum, fluorite, salt rock, carbon dioxide, alum, and water green alum are in dissolved state in the study area, and all of them have not reached saturation. The participation of these minerals in water-rock interaction is the main cause of Ca^{2+}, Mg^{2+}, F^-, Na^+, and Cl^- plasma in groundwater. Carbonate minerals, aragonite, and hematite are dissolved and basically saturated

(4) The water quality index (WQI) shows that the overall water quality situation is good. The irrigation water quality parameters permeability index (PI), magnesium hazard (MH), and Kelly index (KI) indicate that 45.8% of the water samples are "unsuitable." It is mainly concentrated in the coal stratigraphic section, which shows that the water quality of the coal seam is crucial to the utilization of groundwater discharged from the tunnel

Data Availability

The data used to support the findings of this study are included in the article.

Conflicts of Interest

The authors declare that they have no conflicts of interest.

Acknowledgments

This work was supported by the Science and Technology Planning Project of Guizhou Province (Qiankehe Major Special Project [2018] 3011, Qiankehe Basic Project ZK [2022], General Project 082, and Qiankehe Basic Project [2019] No. 1057), Regional First-Class Discipline Construction Project in Guizhou Province (QYNYL [2017] 0013), Guiyang Metro Line 3 Phase I Engineering Research Project (Project No. GD3-FW-YJ-05-2020-13-ZB), and Scientific Research Project of Guiyang Rail Transit Line 2 Phase I Project (Project No. D2(I)-FW-YJ-2019-001-WT).

References

[1] Z. B. Yang, Y. Qin, C. C. Wu, Z. H. Qin, G. Li, and C. L. Li, "Geochemical response of produced water in the CBM well group with multiple coal seams and its geological significance-a case study of the Songhe well group in Western Guizhou," *International Journal of Coal Geology*, vol. 207, pp. 39–51, 2019.

[2] C. Guo, Y. Qin, Y. C. Xia et al., "Geochemical characteristics of water produced from CBM wells and implications for commingling CBM production: a case study of the bide-Santang Basin, western Guizhou, China," *Journal of Petroleum Science and Engineering*, vol. 159, pp. 666–678, 2017.

[3] S. H. Zhang, S. H. Tang, Z. C. Li, Z. J. Pan, and W. Shi, "Study of hydrochemical characteristics of CBM co-produced water of the Shizhuangnan block in the southern Qinshui basin, China, on its implication of CBM development," *International Journal of Coal Geology*, vol. 159, pp. 169–182, 2016.

[4] I. Menéndez Pidal, J. A. Mancebo Piqueras, E. Sanz Pérez, and C. Sáenz Sanz, "Influence of hydrogeochemistry on tunnel drainage in evaporitic formations: El Regajal tunnel case study (Aranjuez, Spain)," *Sustainability*, vol. 13, no. 3, p. 1505, 2021.

[5] X. X. Li, P. Wu, Z. W. Han, X. Zha, H. Ye, and Y. Qin, "Effects of mining activities on evolution of water quality of karst waters in Midwestern Guizhou, China: evidences from hydrochemistry and isotopic composition," *Environmental Science and Pollution Research*, vol. 25, no. 2, pp. 1220–1230, 2018.

[6] Y. R. Lu, "Karst water resources and geo-ecology in typical regions of China," *Environmental Geology*, vol. 51, no. 5, pp. 695–699, 2006.

[7] J. Gisbert, A. Vallejos, A. Gonzalez, and A. Pulido-Bosch, "Environmental and hydrogeological problems in karstic terrains crossed by tunnels: a case study," *Environmental Geology*, vol. 58, no. 2, pp. 347–357, 2009.

[8] H. Li and H. Kagami, "Groundwater level and chemistry changes resulting from tunnel construction near Matsumoto City, Japan," *Environmental Geology*, vol. 31, no. 1-2, pp. 76–84, 1997.

[9] M. Hasegawa, M. Usui, and K. Gotoh, "Geological prognosis ahead of a tunnel face," *Engineering Geology*, vol. 35, no. 3-4, pp. 229–235, 1993.

[10] F. Mossmark, K. K. Annertz, L. O. Ericsson, and M. Norin, "Hydrochemical impact of construction of the western section of the Hallandsås rail tunnel in Sweden," *Bulletin of*

Engineering Geology and the Environment, vol. 76, no. 2, pp. 751–769, 2017.

[11] F. Mossmark, L. O. Ericsson, M. Norin, and L. O. Dahlström, "Hydrochemical changes caused by underground constructions-a case study of the Kattleberg rail tunnel," *Engineering Geology*, vol. 191, pp. 86–98, 2015.

[12] A. Saberinasr, M. Morsali, A. Hashemnejad, and J. Hassanpour, "Determining the origin of groundwater elements using hydrochemical data (case study: Kerman water conveyance tunnel)," *Environmental Earth Sciences*, vol. 78, no. 6, 2019.

[13] M. F. Howladar and M. M. Rahman, "Characterization of underground tunnel water hydrochemical system and uses through multivariate statistical methods: a case study from Maddhapara granite mine, Dinajpur, Bangladesh," *Environmental Earth Sciences*, vol. 75, no. 24, p. 1501, 2016.

[14] N. Ghouili, F. Hamzaoui-Azaza, M. Zammouri, M. F. Zaghrarni, F. J. Horriche, and M. T. Condesso de Melo, "Groundwater quality assessment of the Takelsa phreatic aquifer (Northeastern Tunisia) using geochemical and statistical methods: implications for aquifer management and end-users," *Environmental Science and Pollution Research*, vol. 25, no. 36, pp. 36306–36327, 2018.

[15] Y. Huh and J. M. Edmond, "The fluvial geochemistry of the rivers of Eastern Siberia: III. Tributaries of the Lena and Anabar draining the basement terrain of the Siberian craton and the trans-Baikal highlands," *Geochimica et Cosmochimica Acta*, vol. 63, no. 7-8, pp. 967–987, 1999.

[16] A. F. Khan, K. Srinivasamoorthy, and C. Rabina, "Hydrochemical characteristics and quality assessment of groundwater along the coastal tracts of Tamil Nadu and Puducherry, India," *Applied Water Science*, vol. 10, no. 2, 2020.

[17] A. Roy, T. Keesari, H. Mohokar, D. Pant, U. K. Sinha, and G. N. Mendhekar, "Geochemical evolution of groundwater in hard-rock aquifers of South India using statistical and modelling techniques," *Hydrological Sciences Journal*, vol. 65, no. 6, pp. 951–968, 2020.

[18] Y. A. El-Amier, W. K. Kotb, G. Bonanomi, H. Fakhry, N. A. Marraiki, and A. M. Abd-ElGawad, "Hydrochemical assessment of the irrigation water quality of the El-Salam canal, Egypt," *Water*, vol. 13, no. 17, p. 2428, 2021.

[19] Y. H. Zhou, P. Y. Li, L. L. Xue, Z. H. Dong, and D. Li, "Solute geochemistry and groundwater quality for drinking and irrigation purposes: a case study in Xinle city, North China," *Chemie Der Erde-Geochemistry*, vol. 80, no. 4, p. 125609, 2020.

[20] S. Khalid, "An assessment of groundwater quality for irrigation and drinking purposes around brick kilns in three districts of Balochistan province, Pakistan, through water quality index and multivariate statistical approaches," *Journal of Geochemical Exploration*, vol. 197, pp. 14–26, 2019.

[21] C. D. L. Mora-Orozco, H. Flores-Lopez, H. Rubio-Arias, A. Chavez-Duran, and J. Ochoa-Rivero, "Developing a water quality index (WQI) for an irrigation dam," *International Journal of Environmental Research and Public Health*, vol. 14, no. 5, p. 439, 2017.

[22] World Health Organization, *WHO Guidelines for Drinking-Water Quality*, World Health Organization, fourth edition, 2011.

[23] National standard of the People's Republic of China, *Groundwater quality standard*, 2017.

[24] C. B. Karakus and S. Yildiz, "Evaluation for irrigation water purposes of groundwater quality in the vicinity of Sivas city centre (Turkey) by using GIS and an irrigation water quality index," *Irrigation and Drainage*, vol. 69, no. 1, pp. 121–137, 2020.

[25] Q. M. Wang, S. N. Dong, H. Wang et al., "Hydrogeochemical processes and groundwater quality assessment for different aquifers in the Caojiatan coal mine of Ordos Basin, northwestern China," *Environmental Earth Sciences*, vol. 79, no. 9, 2020.

[26] Z. R. Wang, X. Tian, and X. Wu, "Hydrochemical characteristics and quality assessment of shallow groundwater and CBM co-produced water in the Shizhuangnan block, Qinshui Basin, China," *Environmental Earth Sciences*, vol. 77, no. 3, p. 57, 2018.

[27] R. J. Gibbs, "Mechanisms controlling world water chemistry," *Science*, vol. 170, no. 3962, pp. 1088–1090, 1970.

[28] M. Andres and S. Paul, "Groundwater chemistry and the Gibbs diagram," *Applied Geochemistry*, vol. 97, no. 209-212, pp. 209–212, 2018.

[29] W. Y. Zhang, L. Ma, J. Abuduwaili, Y. X. Ge, G. Issanova, and G. Saparov, "Hydrochemical characteristics and irrigation suitability of surface water in the Syr Darya river, Kazakhstan," *Environmental Monitoring and Assessment*, vol. 191, no. 9, p. 572, 2019.

[30] Z. Y. Wang, Z. Gao, S. Wang et al., "Hydrochemistry characters and hydrochemical processes under the impact of anthropogenic activity in the Yiyuan city, Northern China," *Environmental Earth Sciences*, vol. 80, no. 2, 2021.

[31] H. Xu, Z. H. Hou, Z. S. An, X. Y. Liu, and J. B. Dong, "Major ion chemistry of waters in Lake Qinghai catchments, NE Qinghai-Tibet plateau, China," *Quaternary International*, vol. 212, no. 1, pp. 35–43, 2010.

[32] N. S. Rao, A. Dinakar, M. Sravanthi, and B. K. Kumari, "Geochemical characteristics and quality of groundwater evaluation for drinking, irrigation, and industrial purposes from a part of hard rock aquifer of South India," *Environmental Science and Pollution Research*, vol. 24, no. 24, pp. 31941–31961, 2021.